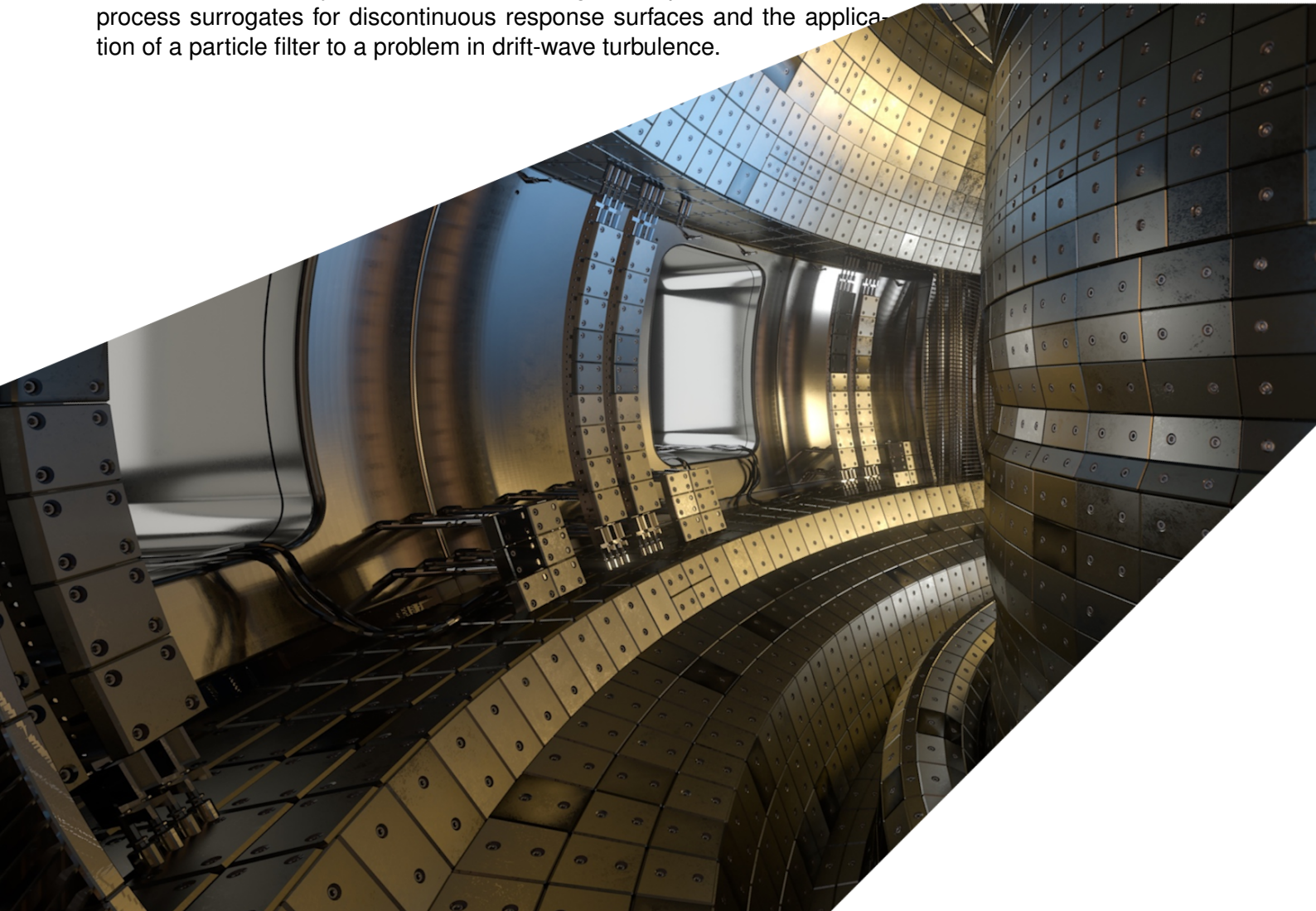# ExCALIBUR

Uncertainty Quantification Complementary Actions: Code Integration, Acceptance and Operation 2

M5c.2 Version 1.00

Abstract

The report describes work for ExCALIBUR project NEPTUNE at Milestone M5c.2. It outlines work towards uncertainty quantification, reduced-order modelling, and data assimilation for NEPTUNE. An analysis of the accuracy of numerical simulations of advection-diffusion problems is presented. Work on the study of the stability of two-dimensional convective flows is described, including a new presentation of the use of solution continuation to elucidate the structure of the Hopf bifurcation from steady flows to time-dependent behaviour. An update on the status of the Smallab fluid heat transfer experiments is given. Work by the holder of the grant T/AW085/21 is briefly summarized, including developments in Gaussian process surrogates for discontinuous response surfaces and the application of a particle filter to a problem in drift-wave turbulence.

UKAEA REFERENCE AND APPROVAL SHEET

	Client Reference:	
	UKAEA Reference:	CD/EXCALIBUR-FMS/83
	Issue:	1.00
	Date:	June 3, 2024

Project Name: ExCALIBUR Fusion Modelling System			

	Name and Department	Signature	Date
Prepared By:	Wayne Arter Ed Threlfall CD	N/A N/A	March 15, 2024 March 15, 2024
Reviewed By:	Owen Parry CD		March 15, 2024

1 Introduction

The uncertainty quantification (UQ) in NEPTUNE is to be non-intrusive, which means that the UQ functionality can be developed largely independently of the main NEPTUNE code base. Since the main NEPTUNE codes are still in development, the first part of this report offers an exposition of accuracy estimation for advection-diffusion problems, which are common in plasma physics generally and NEPTUNE specifically. This analysis is of critical import for the implementation of plasma fluid solvers currently taking place in the NESO framework.

A subject of ongoing relevance for NEPTUNE is heat transfer by a convecting fluid. The stability properties of flows in vertical natural convection were studied in the prequel [1] to the current report, with the discovery in the space parameterized by the Prandtl number and the Rayleigh number of a one-dimensional 'stability frontier' between states with stable steady flows and states which exhibit time-dependent behaviour. This is a little like a phase transition (in that the frontier is a subspace of co-dimension one) and thus would be expected to display collapse to one dimension of the active subspace. Here (§3) a deflated solution continuation analysis is used to give an explanation for the form of the stability frontier as a composite of numerous overlapping instability modes.

The UQ work has been defrayed under Grant T/AW085/21. This grantee's work during the past year has taken the form of code development and related hackathons, and a final written report. This material, which covers UQ, reduced-order models, and data assimilation, is described briefly in §4.

2 Estimating Accuracy in Advection-Diffusion Problems

2.1 Model Problem

This section develops ref [2, § 2.2], concerning discretisations of the time-dependent advection-diffusion equation for a scalar field $f(\mathbf{x}, t)$ in a flow $\mathbf{u}(\mathbf{x}, t)$ with diffusion κ and source term $S(\mathbf{x}, t)$

$$\frac{\partial f}{\partial t} + \nabla \cdot (\mathbf{u} f) = \nabla \cdot (\kappa \nabla f) + S \tag{1}$$

Suppose that f only depends on a single spatial coordinate x, $\mathbf{u}$ has a single component u, and also that the diffusion $\kappa = $ const. Neglecting gradients of $\mathbf{u}$, the analytic model equation may be taken

$$\frac{\partial f}{\partial t} + u \frac{\partial f}{\partial x} = \kappa \frac{\partial^2 f}{\partial x^2} + S \tag{2}$$

Solution is made in the finite domain $0 \leq x \leq L$ over a time interval $[0, T]$. Note that the assumptions made do not exclude the nonlinear case $f = u$, when Equation (2) is known as Burgers equation and κ becomes the viscous diffusion.

It will be important for subsequent work to distinguish different approaches to a dimensionless treatment of Equation (2) and thence Equation (1), see Section 2.2. The following Section 2.3 shows how discretisation of Equation (2) introduces new dimensionless quantities based on mesh spacing, and then Section 2.4 goes on to discuss the implications of these parameters for numerical stability and accuracy. Section 2.3 also includes treatment of the hyper-diffusion term which may be represented as an addition to the source in Equation (2) of form

$$S_4 = -\kappa_4 \frac{\partial^4 f}{\partial x^4} \tag{3}$$

where κ_4 is the hyper-diffusion, *aka* hyper-viscosity in the nonlinear case that $f = u$.

2.2 Dimensionless Parameters

Naturally because of the finite domain, distances are scaled by L, when by far the commonest approach, particularly when $S = 0$ is to make time t dimensionless in terms of the diffusion timescale L^2/κ. It will be recalled that this leads to a model in dimensionless variables of the form

$$\frac{\partial f}{\partial t} + Pe \cdot u \frac{\partial f}{\partial x} = \frac{\partial^2 f}{\partial x^2} \tag{4}$$

where the Peclet number

$$Pe = \frac{U_0 L}{\kappa} \tag{5}$$

with $U_0 = ||\mathbf{u}||$ as a representative absolute value of u, usually the maximum flow-speed. Making t dimensionless in terms of the turnover timescale L/U_0, similarly leads to the appearance of (the reciprocal of) Pe in the coefficient of the diffusion term. The point is that in the linear problem, not only is κ fixed at least in order of magnitude, but also so is u/U_0 similarly of order unity throughout.

3

When u is varying appreciably, eg. in time as a result of instability in a coupled momentum equation (or say due to driving by S when $f = u$), it is often customary to omit the Peclet number, and work with a model in dimensionless variables of the form

$$\frac{\partial f}{\partial t} + u\frac{\partial f}{\partial x} = \frac{\partial^2 f}{\partial x^2} \tag{6}$$

where the dimensionless u may vary over orders of magnitude, and of course even when u is fixed, this formulation is workable. The fixed flow case using the model Equation (6) is then apparently parameter-free, although it should be evident that the scale of the initial values of u serves to set an implicit or 'hidden' Peclet number. (Similar remarks apply in respect of hyperdiffusion upon introducing $Pe_4 = ||\mathbf{u}||h^3/\kappa_4$.)

2.3 Discrete Dimensionless Parameters

Suppose h is the spatial mesh separation implicitly assumed to be uniform, ie. $h = L/N$, where $N + 1$ with $N \gg 1$ is the number of mesh-points in $0 \le x \le L$. Let Δt be the timestep, then the discrete time advance is of general form

$$\frac{\Delta_t f}{\Delta t} + \frac{u}{h}\Delta_x f = \kappa\frac{\Delta_x^2 f}{h^2} \tag{7}$$

where Δ_x and Δ_x^2 are discrete difference operators in the x-coordinate, eg. $\Delta_x f = f_{i+1} - f_i$, operating on the discrete values of f_i at the mesh-points i. (Δ_t is defined analogously.) If $\kappa = 0$ and there is only hyper-diffusion

$$\frac{\Delta_t f}{\Delta t} + \frac{u}{h}\Delta_x f = -\kappa_4\frac{\Delta_x^2 f}{h^4} \tag{8}$$

Evidently the discrete Equation (7) may be made dimensionless using the mesh-scale h, introducing the mesh Peclet number parameter

$$Pe_h = \frac{U_0 h}{\kappa} \tag{9}$$

There are questions concerning the role of Pe_h inherited from a good deal of controversy about the role of the mesh Reynolds number Re_h, viz. Pe_h for the nonlinear case. Nonetheless, at least heuristically it would seem that when $Pe_h = \mathcal{O}(1)$, there is an approximate balance between the *discrete* advective and diffusive terms. For smaller Pe_h the latter dominates, which is numerically significant in that the discrete Laplacian operator, being symmetric and definite, is much easier to treat numerically than the discrete advection operator. (Similar remarks apply to Equation (8) upon introducing

$$Pe_{4h} = \frac{U_0 h^3}{\kappa_4}) \tag{10}$$

Other important well-known dimensionless groups for Equations(7) and (8) are the Courant or CFL number and the diffusion limit parameters, respectively

$$c_h = \frac{U_0 \Delta t}{h}, \quad d_h = \frac{\kappa \Delta t}{h^2}, \quad \text{and} \quad d_4 = \frac{\kappa_4 \Delta t}{h^4} \tag{11}$$

4

When these are separately unity, the corresponding timestep has a simple physical interpretation as respectively the timescale for the turnover, diffusion and hyper-diffusion of one cell of the discretisation. Note also the identities

$$Pe_h = \frac{c_h}{d_h} \quad \text{and} \quad Pe_{4h} = \frac{c_h}{d_4} \tag{12}$$

Note finally that, particularly in the case of more general nonlinear advection-diffusion problems, it is unclear how long the simulated duration T needs to be, and indeed what the smallest physically significant lengthscale will be, thus it is inadequate to consider the simple dimensionless ratios $\Delta t/T$ and $\Delta x/L$.

2.4 Stability Parameters and Accuracy

If the temporal discretisation of Equation (7) is explicit, it is plausible (as is confirmed by rigorous analysis up to factors of order unity) that for stability the timestep must be less than or equal to the turnover and diffusion times of one cell, viz.

$$c_h \leq 1, \quad d_h \leq 1, \quad \text{and/or} \quad d_4 \leq 1 \tag{13}$$

Since maximal size of timestep is to be preferred for computational efficiency, then to within $\mathcal{O}(1)$ factors, $c_h = d_h = 1$ will be taken and so $Pe_h = 1$ at the stability boundary.

It is important to consider accuracy, again this is posed in heuristic terms by assuming that the smallest lengthscale ℓ important in the dynamics of f is capable of numerical estimation, or known say on the basis of analytic results. It follows that for minimally accurate results $h < \ell$. For advection-diffusion problems, whether or not they are linear, provided $S = 0$, then typically

$$\ell = LPe^{-\alpha}, \quad \text{or} \quad \ell_4 = LPe_4^{-\beta} \tag{14}$$

for positive $\alpha \leq 1$ and $\beta \leq 1$. Simple balancing of coefficients gives $\alpha = \beta = 1$, whereas smaller values follow in higher dimensions when the flow is incompressible (typically $\alpha = 1/2$) or from estimates of turbulent microscales in the nonlinear case, giving $\alpha = 3/4$ [3].

Suppose further that hyper-diffusion is added to an advection-diffusion problem for additional numerical smoothing, then it is desirable that the minimum scale h_4 attained by the latter satisfies $\ell_4 < \ell$, equivalently $Pe_4^{-\beta} < Pe^{-\alpha}$, which when $\alpha = \beta$ implies $\kappa_4 < \kappa L^2$, and hence $Pe_4 > Pe_h/N^2$.

Remembering that $L = Nh$ and $Pe = U_0 L/\kappa$, then $h < LPe^{-\alpha}$ gives

$$h < N^{\frac{1-\alpha}{\alpha}} \frac{\kappa}{U_0}, \quad \text{ie.} \quad Pe_h < N^{-1+\frac{1}{\alpha}}, \quad \text{implying} \quad c_h < d_h N^{-1+\frac{1}{\alpha}} \tag{15}$$

Similarly for hyper-diffusion

$$h^3 < N^{\frac{1-3\beta}{\beta}} \frac{\kappa_4}{U_0}, \quad \text{ie.} \quad Pe_{4h} < N^{-3+\frac{1}{\beta}}, \quad \text{implying} \quad c_h < d_4 N^{-3+\frac{1}{\beta}} \tag{16}$$

The results Equations(15) and (16) are key. From Equation (15) it follows that stability of the explicit scheme implies accurate advection-diffusion for all reasonable values of α. Moreover there

is benefit from use of implicit schemes, even on uniform meshes if $\alpha < 1$, since then accuracy is possible even when $c_h \gg 1$.

Whether accuracy is achieved in a time-dependent calculation, depends on the smallest important timescale τ. The work of Hunt et al. [3] implies $\tau = \ell^2/\kappa$, ie. then $\Delta t < \tau$ implies $d_h < 1$ since $h < \ell$ has been assumed, so that temporal accuracy may also be consistent with $c_h \gg 1$. (For hyperdiffusion, $d_4 < \kappa_4/(\kappa h^2)$, so if $\kappa_4 < \kappa L^2$, $d_4 < N^2$.) However if $\tau = \ell/U_0$, which could occur if there were say large initial transients, then for minimal accuracy in the time advance, $\Delta t < \tau$ implies $c_h < 1$. By contrast, in an approach to a steady-state solution, the timescale for change of field variables could become very long, meaning that an implicit scheme would benefit from its ability to take very large timesteps whilst maintaining accuracy.

3 Vertical natural convection revisited

Work described in §3.4 of [1] was performed partially to provide target proxyapps for UQ / ROM / DA investigations as a stand-in until software developed in the NESO framework becomes available for large-scale studies. The aforementioned work targetted the different regimes of vertical natural convection in a square cavity with the aim of providing a 'phase diagram' showing, initially, the dividing line (in a parameter space coordinatized by the two dimensionless parameters in the problems, the Prandtl number (Pr) and the Rayleigh number (Ra)) between convecting systems with a stationary steady-state flow and those where the flow is subject to time-dependent behaviour (this division, which is a Hopf bifurcation, is referred to as the 'stability frontier' in the sequel). This is a very interesting and rich problem due to the variation in the background flow for different values of Pr and Ra . The quantification of behaviour over a wide range of parameters is expected to provide a useful general guide to the behaviour of various fluids in heated cavities: a range of -2 to 2 was used for the base-10 logarithm of the Prandtl number, which covers a wide range of fluids at room temperature e.g. mercury ($\mathrm{Pr} = 0.015$), gases such as air ($\mathrm{Pr} = 0.7$), water ($\mathrm{Pr} = 7.0$), up to viscous oils ($\mathrm{Pr} = 100+$) (this range reflects the relative ease of the diffusive transfer of momentum relative to that of heat). Note the thermal properties of many of these fluids are relevant for fusion-related, as well as more general, engineering applications.

The holder of grant T/AW087/22 was given this problem to further investigate, in order to demonstrate the use of solution continuation techniques; the grantee chose to use the DEFCON software package [4] to apply the technique of deflated continuation to the problem. The deflation technique allows additional solutions to nonlinear systems to be found, basically by removing known solutions from the Newton iteration. The science goals here were to explain the form of the stability frontier, and more prosaically to provide a check on the numerics used in [1] (the grant holder is expert in numerical analysis).

The outcome of the new work is a confirmation of much of the material presented before. The stability frontier was plotted in [1] for two choices of boundary condition on the top / bottom of the cavity (which was coordinatized as a unit square with the bottom left corner at the origin): either conducting, where a an inhomogeneous $(1 - x)$ Dirichlet boundary condition is applied for the temperature (as used in e.g. [5]), or insulating, where a homogeneous Neumann condition applies. Note that the latter case a) appears to exhibit more interesting behaviour and b) is more numerically demanding due to the larger Rayleigh numbers required to trigger time-dependent
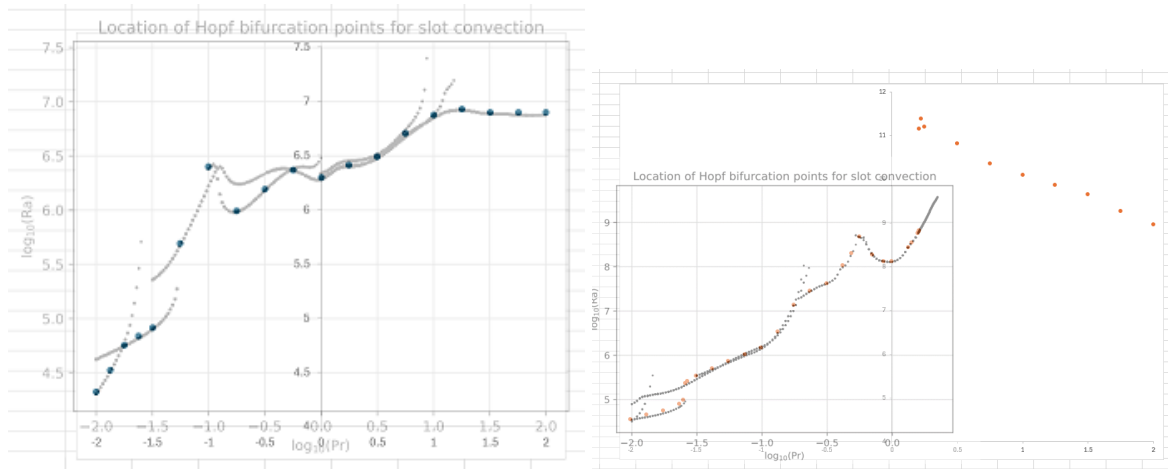
Figure 1: Stability frontiers data produced by grantee (grey points) overlain with data presented in [1]; conducting boundaries (left), insulating boundaries (right).

instabilities (this is an example of the loose rule that a more-insulated fluid system is more likely to remain in a steady flow condition).

The results from [1] are superimposed on the grantee's results in Fig.1. Note the grantee has chosen to transpose the axes relative to the existing work.

The grantee's numerical results for the conducting case shows good general agreement with earlier work over the entire range of parameters studied, with the possible exception of one point at $\log_{10}\mathrm{Pr} = -1$ where the early work appears not to pick up the instability until slightly late into the continuation parameter scan (which used monotonically increasing values of Pr).

The grantee's results for the insulating case show good agreement with earlier work up to $\log_{10}\mathrm{Pr} \approx 0.4$. For higher Pr values, where the numerics are more challenging due to the narrowness of the boundary layers on the upright walls, the grantee was unable to obtain numerical results to the same level of precision as their other results. Indeed, their results for lower precision (the continuous part of the grey curve in Fig.1 and the continuous dark blue curve in Fig.2) show marked discrepancy with the numerical results presented in [1]. In view of the interesting behaviour seen in the latter, this is slightly unfortunate and further study of this region of parameter space for the problem would appear to be indicated. The author considers their earlier results in need of further verification (note also the discrepancy with the study by Wang et al [6] for $\log_{10}\mathrm{Pr} = 1.0$ exhibited in Fig.14 of [1]). Nevertheless, the grantee's work has provided a verification of a large portion of the parameter space for the stability frontier.

Rather informative colour-coded versions of the stability frontier diagrams were produced by the grantee (Fig.2), showing that the frontier is in both boundary condition cases a composite of multiple instabilities protruding into the steady-flow part of the parameter space. This structure means that the frontier is a continuous curve with points of discontinuous derivative (cusps). It would be of interest to obtain a plot of the instability mode associated to each of the solution branches.

The grantee's work was presented in-person (at the NEPTUNE Workshop 2024) in lieu of a written report. The associated proxyapp code and some documentation can be accessed in the repository
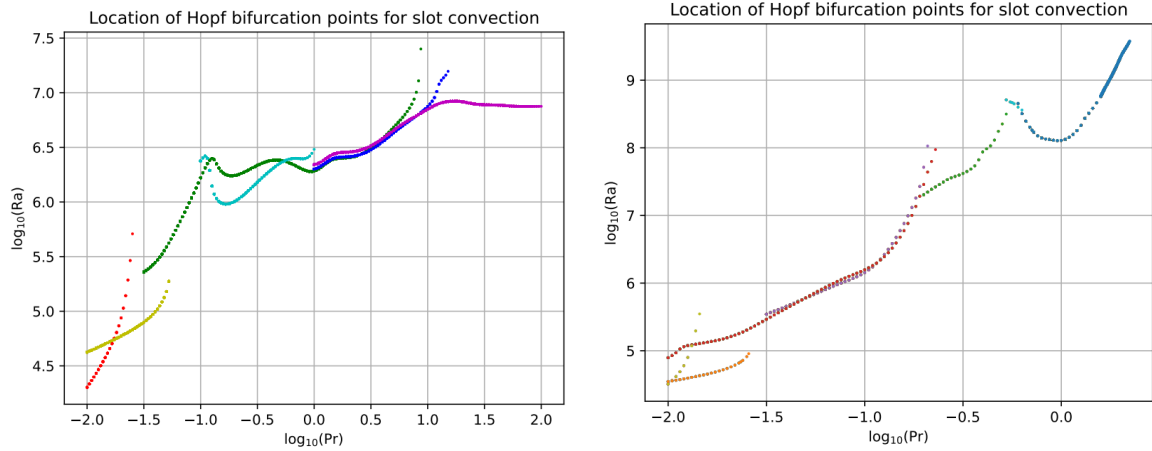
Figure 2: Stability frontiers colour-coded by solution branch; conducting boundaries (left), insulating boundaries (right). Different branches denote different time-dependent instabilities. Note that the continuous blue curve to the extreme right of the right-hand-side plot is a numerical region where the precision needed to be reduced due to the numerical demands of the large Rayleigh number and this part of the plot does not agree with the results reported in [1].

[7]. Note that this code was based on the Firedrake scripts used in the earlier study but that the grantee extended it to use the DEFCON software to track the solution branches and therefore the original code has now been inspected by more than one professional numerical analyst.

The present author is very interested to know whether any results are available regarding the overall shape of the stability frontier or any asymptotics (e.g. very small or very large Pr or Ra). There are many possibilities for further work, involving extension of the studied parameter ranges, and extension into other geometries including the three-dimensional case which is expected to contain additional instabilities.

The same grantee performed related work applying adjoint methods to the cavity problem for values of Ra near the stability frontier, in the case of air as the fluid ($\mathrm{Pr} = 0.71$ / $\log_{10}\mathrm{Pr} = -0.15$, which falls within the region where there is agreement between numerics of the author and those explained above). This work used the adjoint analysis features available in Nektar++, thus providing a useful example of an adjoint problem in Nektar++ (which latter is the finite-element framework currently used as a basis for the NESO plasma fluids solvers). In this case, the adjoint analysis is used to discover the perturbations in the wall temperatures profiles to which the system is most sensitive, which is complementary to the stability frontier work which concerns currently only constant vertical wall temperatures. This work was reported as Technical Report 2068625-TN-09, and the code and scripts used (including some new additional Nektar++ source code) can be found at [8].

3.1 Additional physics of vertical natural convection

The vertical natural convection problem has other interesting aspects beyond the physics of the transition to time-dependent behaviour. One is of course the turbulent regime, but even the laminar

8

flows exhibit a range of physical effects that are the subject of current investigation by the fluids community; an example of the latter is the study of secondary flows in [9] (which does not include any UQ analysis). It might be noted that, while continuation in Pr, which is a property of the fluid, may not seem particularly physically-motivated, it is actually the case that many fluids exhibit significant change in Pr as their temperature is varied.

The examples in Fig.3 were run using Firedrake to find the steady flow in a tall tank (aspect ratio 10). The code solves initially the problem for a value of the Prandtl number close to unity, which flows are a single convective cell and prove numerically easy to obtain. Subsequently, continuation is performed i.e. Pr is gradually decremented and the simulation is re-run using the previous solution as an initial guess. This reveals, for sufficiently small values of Pr, more interesting flow patterns containing multiple convective cells along the tank length resulting in an approximate periodicity, and which may display more than one cell structure per period (i.e. the alternating-size sawtooth pattern seen in the left-hand figure).

The utility of the above in a UQ / ROM context is that these flows could be made the subject of a campaign of simulations where the objective is to develop a smart choice of 'experimental design' (i.e. choosing where in parameter space to perform simulations for use in surrogate construction) including the need for solution continuation (which means that new simulations in some areas of parameter space must use a nearby solution as an initial guess in order to obtain convergence; see the discussion in §.3 of [1]). Such work would extend the grantee's current expertise in experimental design.

It is clearly also possible to do the stability frontier analysis on this sort of tank geometry.

4   Management of grant T/AW085/21

The present author has been responsible for the management of the titular grant for approximately the past year. This has included regular online meetings to discuss the grant work and also regular attendance at the meeting series 'Uncertainty in Fluid Turbulence' chaired by Professor Peter Coveney of University College London. As has previously been the case, the utility to Project NEPTUNE of the grantee's expertise and technology (which includes the SEAVEA Toolkit of uncertainty quantification software (the acronym stands for Software Environment for Actionable and VVUQ-evaluated Exascale Applications), and also other powerful frameworks as listed in §.5 of [10]) has been affected by the lack of a large-scale plasma solver code within the NEPTUNE software ecosystem. It has been a priority to ensure that such a code is developed, hence the implementation of working plasma solvers in the NESO framework (these were described in [11]).

Another area of work relevant to this grant is the Smallab fluid tank experiment being developed at Leeds University. It was originally conceived that novel measurements from such experiments would form the basis for data assimilation and reduced-order modelling work under NEPTUNE, leading towards a digital twin of a tabletop fluid heat transfer experiment. Unfortunately, there are as yet no meaningful measurements from the experiment, which the present author understands to have been delayed as a result of practical difficulties (and said author in no way wishes to understate the challenges of this experiment). Note that the experimental work is being supported by numerical simulation performed using, among other softwares, Nektar++, including efforts by
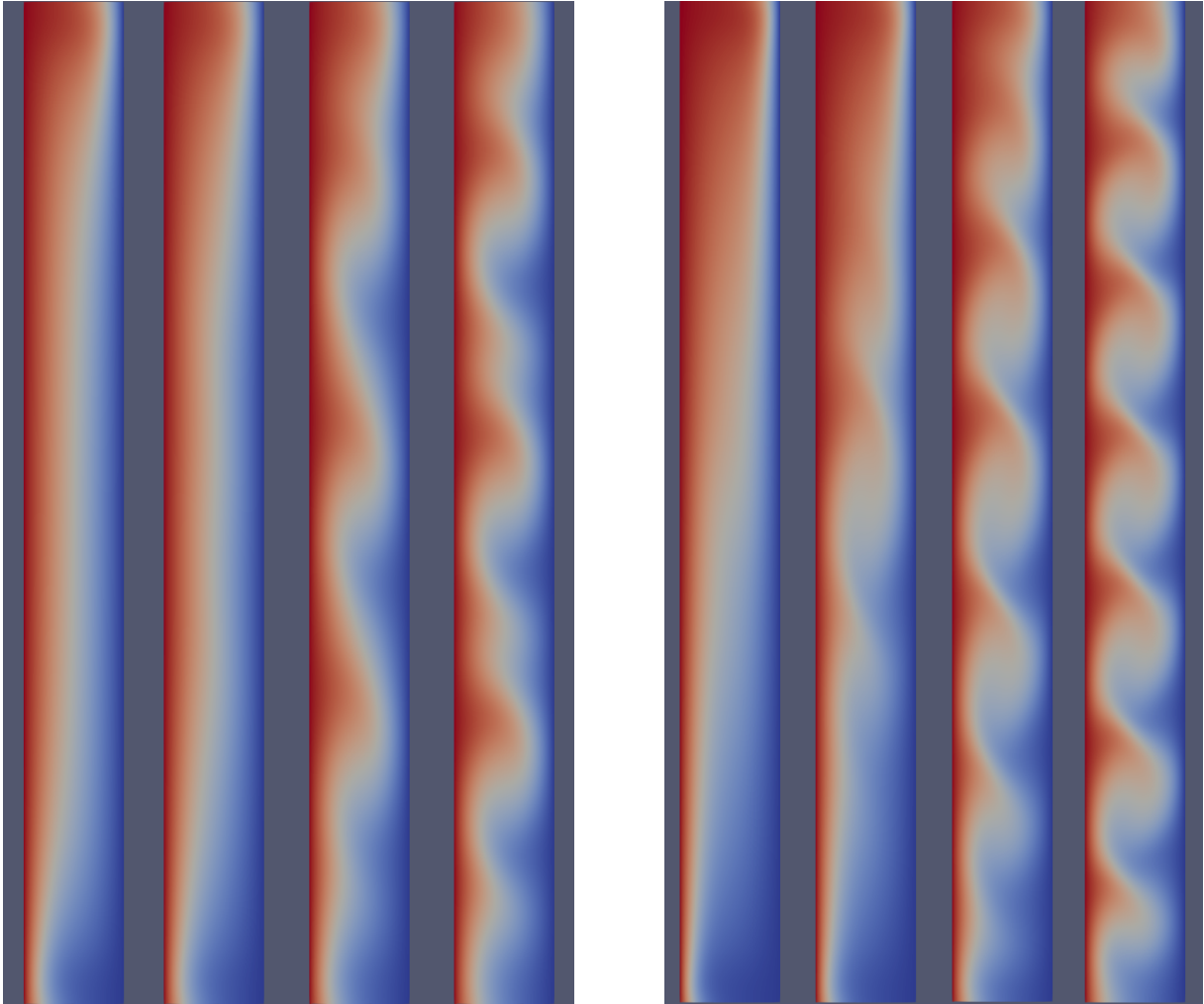
Figure 3: Steady-state temperature colour maps for laminar flows. Left panel: $\log_{10}\mathrm{Ra} = 3.5$; $\log_{10}\mathrm{Pr} = -0.1, -0.4, -0.7, -1.0$ (left to right). Right panel: $\log_{10}\mathrm{Ra} = 4.0$; $\log_{10}\mathrm{Pr} = -0.2, -0.6, -1.0, -1.4$ (left to right). The acceleration due to gravity acts (as usual) in the down-ward direction.
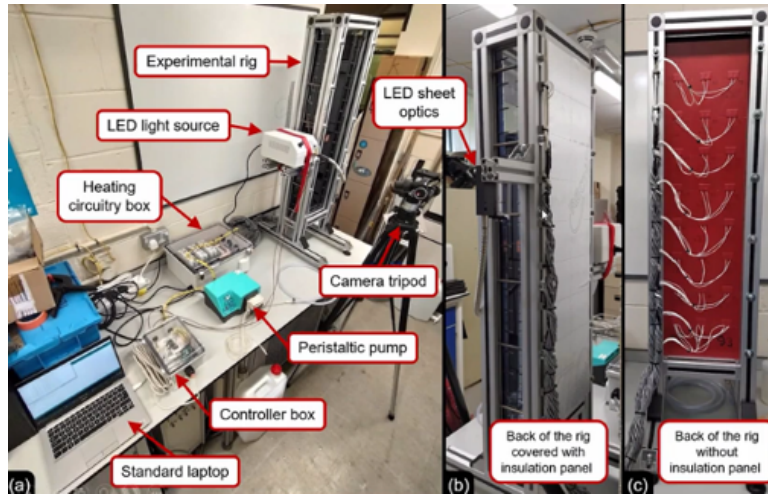
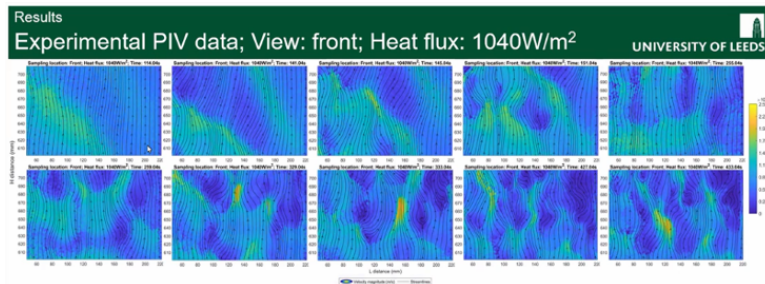Figure 4: Labelled experimental setup for Smallab fluid tank experiment.

Figure 5: Example velocimetry outputs from an early version of the Smallab fluid tank experiment. The colour map indicates the local flow speed.

the experimenter and also fully 3D numerics performed by UKAEA personnel (for the latter see Fig.17 of [1]). An image of the apparatus being considered is shown in fig 4, from which some of the complexity involved is apparent. The experimenter has given a preliminary presentation detailing the experiment design and showing some initial measurements (e.g. Fig.5); a video recording of this presentation exists and may be available, subject to relevant permissions, by appealing to the authors of this report.

The holder of grant T/AW085/21 has continued to provided HPC allocations on Archer2 to some of the other grantees (specifically, the holders of grants T/AW087/22 and T/AW088/22) and to the UKAEA, which latter allowance continues for at least three months after the expiry of T/AW085/21.

Further details of the work described in this section can be found in UCL grantee report 2057701-TN-02 [12].

4.1 NESO

The grantee has implemented a plugin for FabSim3 to facilitate HPC runs of UKAEA NESO software. This is currently set up with turn-key examples including a polynomial chaos expansion of outputs from the existing 2D-in-3D Haswgawa-Wakatani plasma solver in NESO and a Bayesian calibration run using the NESO Electrostatic2D3V solver.

4.2 Reduced-order models for discontinuous response surfaces

Many models relevant to fusion exhibit discontinuous response surfaces (examples are the transition to a convecting state in Rayleigh-Bénard convection in a continuum fluid when the problem is parameterized by Rayleigh and Prandtl numbers, and the various steady-states of the two-stream instability in the space parameterized by the plasma frequency and the proper velocity of the initial beams - see Appendix A.3 of [13]). Note that the two-stream instability is a model problem in plasma continuum kinetics and has formed the basis for one of the NEPTUNE proxyapps developed under the grant T/AW084/21. It is well-known that standard Gaussian process (GP) techniques work well for smooth response surfaces and the grantee has explored the performance of GP surrogates for the discontinuous response case. The model chosen was the Lorenz 63 reduction of Rayleigh-Bénard convection to a set of nonlinear ODEs. Like the full problem, this system has a parameter space coordinatized by the Prandtl and Rayleigh numbers. The response is taken to be the Nusselt number (which in the full problem is the rate of heat transfer across the convecting fluid). The Nusselt number exhibits discontinuous behaviour in $(\mathrm{Ra}, \mathrm{Pr})$-space (Fig.6) because some choices of these parameters means the system tends to a stable fixed point, whereas other values lead to the chaotic behaviour associated to the familiar Lorenz attractor.

The grantee investigated this problem using a two-layered deep GP and a Latin hypercube-based design for selecting new sampling points in $(\mathrm{Ra}, \mathrm{Pr})$-space. Further, due to the knowledge of the asymptotics, rectangular regions were selected as bounding boxes for the asymptotes, giving two subregions in which to conduct Latin hypercube sampling; in this way, the sample points are concentrated near where the discontinuity is expected to be. This may reasonably be described as a physics-informed experimental design method. Note that the method relies on knowing in advance the asymptotes of the stability frontier. The grantee has developed also a statistical method capable of estimating where the gradient in the underlying model exceeds a certain threshold and some outputs can be seen in Fig.7.

Note that the two-stream instability cases show a markedly similar structure to that seen in the Lorenz 63 model with an L-shaped stability frontier having two linear asymptotics (Fig.8). In the figure, ω_P is the plasma frequency, the counter-propagating beams have initial speeds $\pm v_0$ and Gaussian width (i.e. square root of temperature) σ and k is just a constant. The equation for the stability frontier is $y \equiv \frac{\omega_P}{k\sigma} = (2xD_+(x) - 1)^{-\frac{1}{2}}$ where $x \equiv \frac{v_0}{\sqrt{2}\sigma}$ and $D_+(x) \equiv \frac{\sqrt{\pi}}{2}e^{-x^2}\mathrm{erfi}(x)$ is a Dawson function. The two linear asymptotes are $x = 0.92414$ and $y = \sqrt{2}x$.
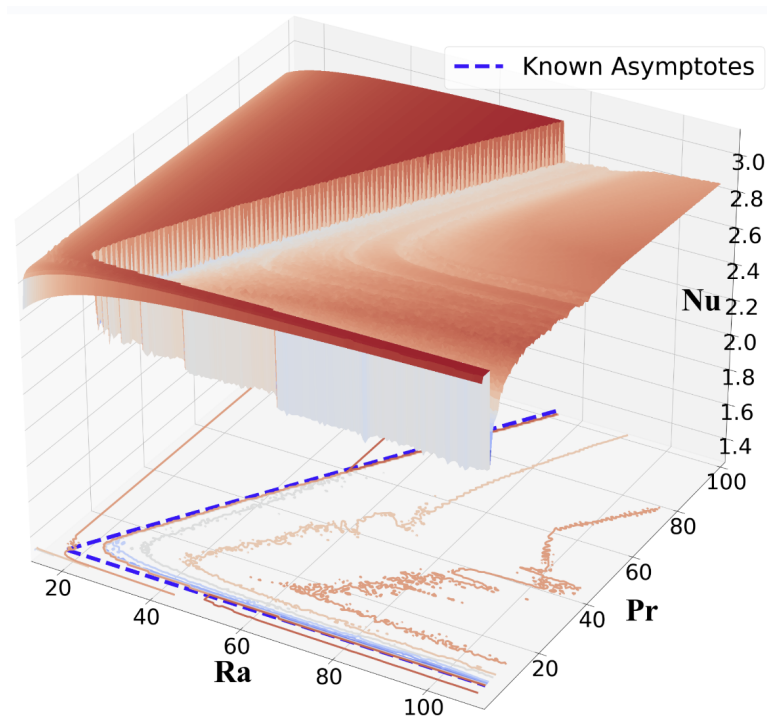
Figure 6: Response surface i.e. Nusselt number (Nu) as a function of Rayleigh (Ra) and Prandtl (Pr) numbers for the Lorenz 63 system. The dashed blue lines are the known linear asymptotes of the stability frontier (given by the discontinuity in the response surface).
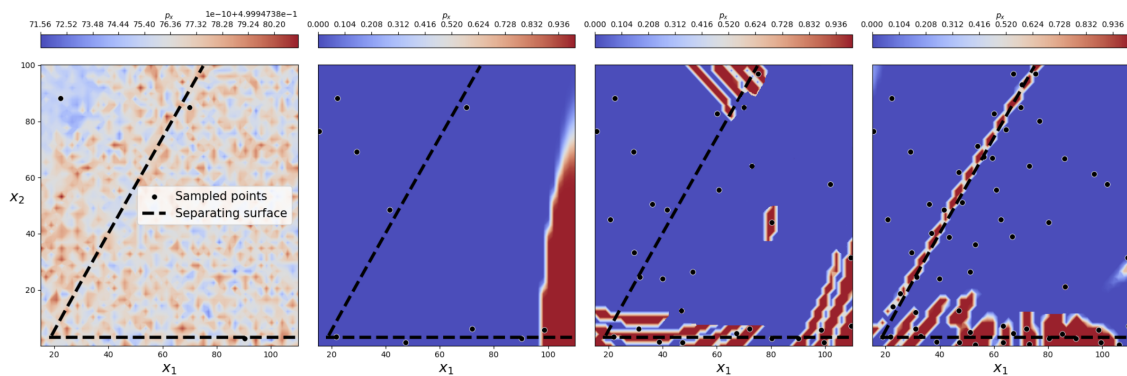

Figure 7: Sequential design for numerical experiments designed to detect the discontinuity in the response surface discussed in the text. The colourmap indicates the probability that the local gradient exceeds a threshold value. The surface estimates shown used 3, 10, 30 and 50 samples (increasing left to right).
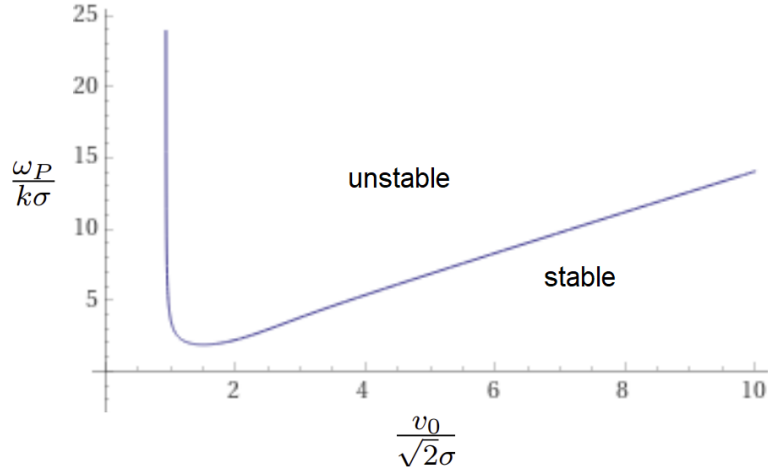
13

Figure 8: Stability frontier for the two-stream instability problem.

4.3 Data assimilation: initial study of drift-wave turbulence

A particle filter-based data assimilation package, *ParticleDA.jl* [14], was released during 2022. An initial version, which provides data assimilation capability linked to the other capabilities of the *SEAVEA Toolkit*, can be found at [15]. One of the author's goals has been to apply this particle filter implementation to some of the proxyapps developed under NEPTUNE. The output of the Nektar++-based proxyapp Nektar-Driftwave was chosen as an initial target and the problem setup was started at a SEAVEA hackathon event which occurred on December 1, 4-5 2024 and was attended by two personnel from UKAEA NEPTUNE.

As background, the filtering problem is typically of the form

$$
\begin{aligned}
X_k &= g(X_{k-1}) + W_{k-1} \\
Y_k &= h(X_k) + V_k.
\end{aligned}
\tag{17}
$$

In the above, X_k is the state of the system at time horizon k and Y_k is an observation. W_{k-1} is the stochastic component of the model update and V_k is measurement noise associated to observation k. The model update is g and is Markov. The goal is to estimate the posterior distribution of the model state given the measurements. Note that for a linear update g and Gaussian W_k and V_k this posterior is available analytically and this is the usual Kalman filter treatment. The particle filter is a way of doing this problem that works in nonlinear cases such as Nektar-Driftwave.

Since all currently-available NEPTUNE / NESO proxyapps are deterministic, and no experimental results are available (results from the fluid tank experiment mentioned in §.3 would have served admirably), the particle filter must be applied to proxyapp outputs to which some artificial noise is added (particle filters require a non-degenerate distribution of state at future times given the current state). The grantee implemented a method of generating Gaussian random fields on a spatial domain, within the Nektar++ framework, and this Gaussian noise was added to simulation outputs to simulate model error.

14

It is worth noting that the version of Nektar-Driftwave used by the grantee has, subsequent to this work, been updated and is now a great deal faster (i.e. at least one order of magnitude) in execution than before. The simulations used here were run on HPC but it is likely now that this work could be reproduced quickly using only a laptop.

Outputs are shown in Fig.9. The filter is found to work adequately for early times, but once the simulation starts to enter the turbulent state, the method fails due to the well-known degeneracy problem of particle filters, that is, the weights for most of the particles drop to near-zero, making the ensemble close to degenerate. The grantee proposes improved proposal distributions and / or use of localization as possible improvements (it is also the case that increasing the ensemble size (i.e. the number of particles) would stave off the degeneracy problem and allow the state to be tracked for a longer time).

It would probably be better to apply the filter to one of the other outputs of the model which have a smoother general appearance than the vorticity, e.g. the potential, which obeys $\nabla^2 \phi = w$ (it is clear that differentiating twice results in a less-smooth function, and in the numerical implementation the potential is a continuous field, while the vorticity and density use a discontinuous representation).

The problem discussed here is rather similar to an application of a particle filter to the barotropic vorticity equations, detailed in Ch.13 of [16], in particular §.13.4.7. That analysis gives some possible methods for improving the initial results . Note that in this example, the vorticity field seems to have been chosen as the target for the data assimilation problem in order to give a more-challenging task than would be the case if the streamfunction (the equivalent of the potential in the Nektar-Driftwave case) were used.

$$
\begin{aligned}
\frac{\partial w}{\partial t} - \frac{\partial \psi}{\partial y}\frac{\partial w}{\partial x} + \frac{\partial \psi}{\partial x}\frac{\partial w}{\partial y} &= \beta \\
\frac{\partial^2 \psi}{\partial x^2} + \frac{\partial^2 \psi}{\partial y^2} &= w
\end{aligned}
\tag{18}
$$

Here w is the vorticity, ψ the streamfunction, and β a random noise term representing errors in the model equations. These equations are very similar to the 2D Hasegawa-Wakatani system modelled by Nektar-Driftwave.

Unfortunately, the current implementation of NESO-Particles does not allow for stochastic time-evolution i.e. there is no stochastic input to the model once it is started (i.e. a run, once initialized, is deterministic). This means NESO-Particles simulations cannot yet be used with the particle filter. This issue will go away once Monte Carlo collisions are available in NESO-Particles.
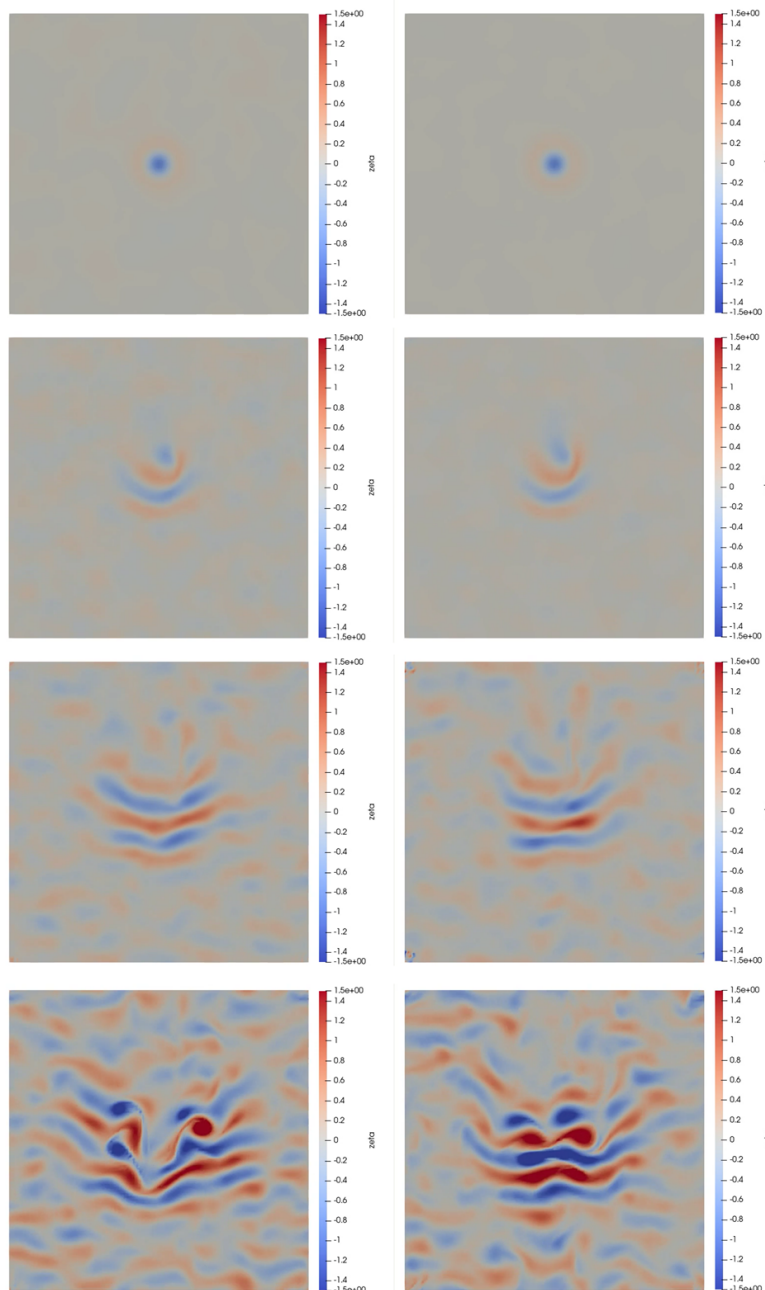
Figure 9: Time-evolution of the vorticity in Nektar-Driftwave: true state (left) and particle filter estimate of the mean using an initial ensemble size of 512 particles. The state is tracked well during the initial evolution but fails later on due to the degeneracy problem.

5 Summary

Material for understanding the numerical errors associated to advection-diffusion problems, which problems are ubiquitous in simulations of plasma physics, was presented.

An update to the analysis of stability for 2D convecting fluid problems, started in [1], was provided and an explanation for the form of the stability frontier curve was presented.

The recent work of the holder of grant T/AW085/21 on uncertainty, reduced-order models, and data assimilation was briefly summarized.

The authors acknowledge assistance from Niall Bootland, Ubaid Qadri and Josh Williams of STFC, and Peter Coveney, Matt Graham, Serge Guillas, Yiming Yang and others of University College London.

Acknowledgement

References

[1] E. Threlfall and Powell S. Complementary actions: uncertainty quantification code integration, acceptance, and operation 1. Technical Report CD/EXCALIBUR-FMS/0073, UKAEA Project Neptune.

[2] W. Arter. Numerical simulation of magnetic fusion plasmas. *Reports on Progress in Physics*, 58:1–59, 1995. `http://dx.doi.org/10.1088/0034-4885/58/1/001`.

[3] J.C.R. Hunt, I. Eames, J. Westerweel, P.A. Davidson, S. Voropayev, J. Fernando, and M. Braza. Thin shear layers-the key to turbulence structure? *Journal of Hydro-environment Research*, 4(2):75–82, 2010.

[4] DEFCON code Bitbucket repository. `https://bitbucket.org/pefarrell/defcon/src/master/`. Accessed: March 2024.

[5] Winters K.H. Hopf bifurcation in the double-glazing problem with conducting boundaries. *Transactions of the ASME 894 / Vol.109, November 1987.*, 1987.

[6] Wang Q., Liu H-R., Verzicco R., Shishkina O., and Lohse D. Regime transitions in thermally driven high-Rayleigh number vertical convection. *J. Fluid Mech. (2021) Vol.197 A.6 doi:10.1017/jfm.2021.262*, 2021.

[7] NumericalAnalysis/Continuation code repository. `https://github.com/ExCALIBUR-NEPTUNE/NumericalAnalysis/tree/main/Continuation`. Accessed: March 2024.

[8] NumericalAnalysis/Adjoint code repository. `https://github.com/ExCALIBUR-NEPTUNE/NumericalAnalysis/tree/main/Adjoint`. Accessed: March 2024.

[9] Umbria J.S. and Net M. Prandtl number dependence of convective fluids in tall laterally heated slots. *The European Physics Journal Special Topics Vol. 227*, pages 481–492, 2018.

[10] E. Threlfall, S. Powell, and W. Arter. Complementary actions. Uncertainty Quantification Code integration, acceptance and operation 1. Technical Report CD/EXCALIBUR-FMS/0073-M5c.1, UKAEA, 3 2023. `https://github.com/ExCALIBUR-NEPTUNE/Documents/blob/main/reports/ukaea_reports/CD-EXCALIBUR-FMS0073-M5c.1.pdf`.

[11] J. Cook, W. Saunders, and O. Parry. Three-Dimensional integrated particle and continuum model. Technical Report CD/EXCALIBUR-FMS/0079-M4c.3, UKAEA, 9 2023. `https://github.com/ExCALIBUR-NEPTUNE/Documents/blob/main/reports/ukaea_reports/CD-EXCALIBUR-FMS0079-M4c.3.pdf` to be posted.

[12] S. Guillas. Advanced Quantification of Uncertainties In Fusion modelling at the Exascale with model order Reduction (AQUIFER) 2. Technical Report 2057701-TN-02, UKAEA Project Neptune, 2024. to be posted at `https://github.com/ExCALIBUR-NEPTUNE/Documents/blob/main/reports/2057701/TN-02.pdf`.

[13] Arter W., Parry O., and E. Threlfall. Finite element models: complementary actions 3. Technical Report CD/EXCALIBUR-FMS/0074, UKAEA Project Neptune.

[14] ParticleDA.jl. `https://github.com/Team-RADDISH/ParticleDA.jl`. Accessed: March 2023.

[15] FABParticleDA. `https://github.com/djgroen/FabParticleDA/tree/master`. Accessed: March 2023.

[16] Blayo É., Bocquet M., Cosme E., and Cugliandolo L.F. *Les Houches 2012: Advanced Data Assimilation for Geosciences*. Oxford University Press, 2015.